Available online at www.sciencedirect.com
ScienceDirect
Catalysis Communications 8 (2007) 834–838
CATALYSIS COMMUNICATIONS
www.elsevier.com/locate/catcom

Preparation and characterization of nanostructured $Ce_{0.9}Cu_{0.1}O_{2-\delta}$ solid solution with high surface area and its application for low temperature CO oxidation

Meng-Fei Luo [a,*], Yu-Peng Song [a,b], Xiang-Yu Wang [b], Guan-Qun Xie [a], Zhi-Ying Pu [a], Ping Fang [a], Yun-Long Xie [a]

[a] *Zhejiang Key Laboratory for Reactive Chemistry on Solid Surfaces, Institute of Physical Chemistry, Zhejiang Normal University, Jinhua 321004, China*
[b] *Department of Chemistry, Zhengzhou University, Zhengzhou 450052, China*

Received 4 August 2006; received in revised form 14 September 2006; accepted 16 September 2006
Available online 23 September 2006

Abstract

Nanostructured $Ce_{0.9}Cu_{0.1}O_{2-\delta}$ solid solution with high surface area was prepared by improved citrate sol–gel method with incorporation of thermal treatment under N_2. The sample was characterized by TG–DSC, BET nitrogen adsorption, XRD and H_2-TPR. Its catalytic activity for CO oxidation was tested. It was found that the improved method offered catalysts with higher surface area and smaller crystallite size, which led to higher catalytic activity for low temperature CO oxidation. H_2-TPR measurement indicated that there were three CuO species in the $Ce_{0.9}Cu_{0.1}O_{2-\delta}$ solid solutions: finely dispersed CuO species on the surface of CeO_2, partial Cu^{2+} penetrated into CeO_2 lattice and bulk CuO phase. The finely dispersed CuO species was regarded as the active site for the low temperature CO oxidation.

Keywords: $Ce_{0.9}Cu_{0.1}O_{2-\delta}$ solid solution; Sol–gel method; Nanostructure; High surface area; CO oxidation

1. Introduction

Cerium oxide and its modified derivatives have been widely studied in recent years due to their high activity for oxidation reactions [1–6]. A convincing example is CuO–CeO_2, which is efficient for the CO oxidation at low temperature [7–10]. Due to this promising advantage, CuO–CeO_2 is expected to substitute the noble metal base catalysts in the future [9]. For years, nanostructure has attracted great attention due to its unusual electrical, chemical and catalytic properties [11,12]. Particularly, the nanostructured particles with high surface area provide much more active sites [1]. In the previous research, it has been demonstrated that the nanocrystalline nonstoichiometric Ceria exhibits significantly improved catalytic properties at lower temperature compared with their coarse-grained counterpart [4]. The rate of CO oxidation on Au particles, supported on nanocrystalline CeO_2 was found to be 100 times higher than that reaction on regular CeO_2 support [13].

For the last two decades, the citrate sol–gel method has become one of the popular techniques for preparing metallic oxide materials with high specific surface area and homogeneous distribution [14]. Recently, Chen et al. modified the conventional citrate precursor method by incorporating a nitrogen protection step before the citrate precursors were calcined in air, and nanosized MgO particles with high specific surface area were obtained [15]. Xie et al. prepared $Ce_{0.8}Pr_{0.2}O_Y$ solid solution with ultrafine crystalline sizes and high specific surface area according to the improved method [2].

In this paper, $Ce_{0.9}Cu_{0.1}O_{2-\delta}$ solid solution with high surface area was prepared by the similar method. As a

* Corresponding author. Tel.: +86 579 2283910; fax: +86 579 2282595.
E-mail address: mengfeiluo@zjnu.cn (M.-F. Luo).

1566-7367/$ - see front matter © 2006 Elsevier B.V. All rights reserved.
doi:10.1016/j.catcom.2006.09.017

comparison, other samples were also prepared by conventional method. It demonstrated that the Cu catalyst supported on high surface area CeO_2 showed higher activity for CO oxidation than the conventionally prepared CeO_2 with low surface area.

2. Experimental

2.1. Catalyst preparation

$Ce_{0.9}Cu_{0.1}O_{2-\delta}$ solid solutions were prepared by two citrate sol–gel methods, using Ce $(NO_3)_3 \cdot 6H_2O$ and Cu $(NO_3)_2 \cdot 3H_2O$ as the starting materials.

Conventional citrate sol–gel method (the conventional method): A mixture of Ce $(NO_3)_3 \cdot 6H_2O$ and Cu $(NO_3)_2 \cdot 3H_2O$ with a molar ratio of Ce:Cu = 9:1 was dissolved into deionized water. Then citric acid was added with two times molar amounts to the premixed solution of cerium and copper nitrate while stirring. After that, the solution was heated in water bath until a viscous gel was obtained. In this process, the mixture color turned from blue to green. The gel was dried at 110 °C overnight for the formation of a spongy material, i.e. $Ce_{0.9}Cu_{0.1}O_{2-\delta}$ citrate precursor. This precursor was directly calcined in air at 400 °C or 800 °C for 4 h, denoted as A4 or A8, respectively.

Improved citrate sol–gel method (the improved method): $Ce_{0.9}Cu_{0.1}O_{2-\delta}$ citrate precursor was prepared in the same procedure as mentioned in the conventional method. Then the precursor was put in a tube furnace and heated in the nitrogen atmosphere at 800 °C for 2 h to result in a black mixture of CuO–CeO_2 and carbon powders (the intermediate mixture), denoted as N8. Subsequently, the intermediate mixture (N8) was calcined in air at 400 °C for 4 h to burn the carbon species, denoted as N8A4.

2.2. Catalyst characterization

TG–DSC experiments of the intermediate mixture (N8) were performed using a Netzsch STA 449C instrument. Since the sample may fly off during the thermal analysis, all the samples were prepared by crimping a known amount of sample in an aluminum pan with a lid having a hole (to vent off the evolving gases). The experiments were carried out to a maximum temperature of about 800 °C with a heating rate of 5 °C min^{-1} in air with a flow rate of 50 ml min^{-1}.

X-ray diffraction (XRD) patterns were collected on a Philips PW3040/60 automated powder diffractometer, using Cu Kα radiation ($\lambda = 0.1542$ nm). The working voltage of the instrument was 40 kV and the working current was 40 mA. The intensity data were collected at room temperature over a 2θ range of 20–90° with a scan rate of 1.2° min^{-1}.

Nitrogen adsorption–desorption isotherms were obtained at 77 K on an Autosorb-1 apparatus. BET and BJH method were used to determine the surface area and pore size distribution of the samples.

The reducibility of CuO–CeO_2 catalysts were measured by hydrogen temperature-programmed reduction (H_2-TPR). A 10 mg of sample was placed in a quartz reactor which was connected to a conventional TPR apparatus and the reactor was heated from 100 °C to 900 °C with a heating rate of 20 °C min^{-1}. The reaction mixture was consisted of 5% H_2 and 95% N_2. The amount of H_2 uptake during the reduction was measured by thermal conductivity detector (TCD).

2.3. Catalytic activity measurement

The catalytic activity measurement was carried out in a fixed bed reactor. The catalysts were pressed to pellets, crushed and sieved to 20–40 mesh. A 500 mg of catalyst was used for reaction without any pretreatment. In the reaction, the total gas flow rate was 80 ml min^{-1}, corresponding to a space velocity (S.V.) of 10,000 h^{-1} and the reaction was stabilized for 1 h at each temperature. The composition of inlet gas mixture was 3% CO, 3% O_2 in volume and with N_2 as balance gas. The inlet and outlet gas mixtures were analyzed on an Agilent 6850 gas chromatograph equipped with a TCD detector attached with a HP PLOT column (30 m × 0.32 mm × 12.0 μm).

3. Results and discussion

3.1. Characterization of catalysts

Fig. 1 shows the TG–DSC curves of sample N8. A main weight loss was observed between 200 °C and 350 °C and was about 15% with regard to the total weight of the sample N8, accompanied by a strong exothermic peak at 280 °C, which can be primarily attributed to the combustion of carbon species. Thermal analysis results also indicated that the carbon species in samples N8 could be completely removed after calcination at 400 °C in air. Since

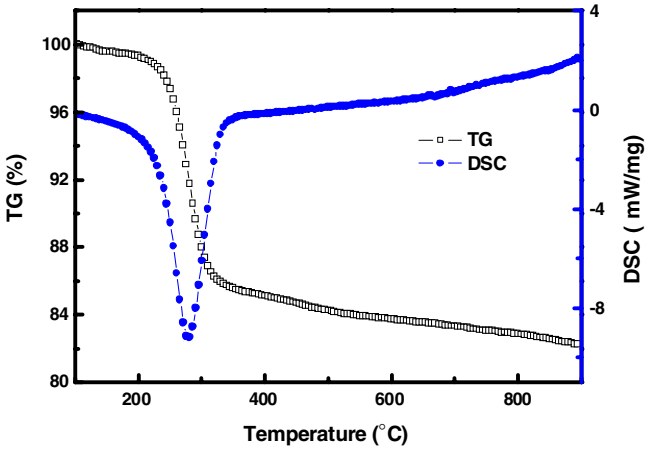

Fig. 1. TG–DSC curves of sample N8.

calcination at high temperature could result in decline in the surface area and increase in the crystallite size of catalysts [1,16], the feasible calcination temperature under air atmosphere was 400 °C.

N_2 adsorption–desorption isotherms of sample N8A4, A4 and A8 were shown in Fig. 2. N8A4 displayed a hysteresis loop with a sloping adsorption branch and a relatively steep desorption branch at a medium pressure ($P = 0.4$–$0.5P_o$), which was typical of type IV (IUPAC classification), and characteristic of inorganic porous oxides. A4 also exhibited a hysteresis loop but with a smaller sloping adsorption branch, while the hysteresis loop was hardly seen on A8. The pore size distributions were obtained according to the BJH method using Halsey equation for multilayer thickness. The adsorption pore size distribution of sample N8A4 was in the narrow range between 1.0 nm and 9.0 nm (inset of Fig. 5), while those of samples A4 and A8 were much broader. The specific surface areas of all samples determined by BET were summarized in Table 1. The specific surface area of sample N8A4 was 131 $m^2\,g^{-1}$, which was much larger than those of samples A4 and A8 (60 $m^2\,g^{-1}$ and 10 $m^2\,g^{-1}$). The specific area decreased with increasing calcination temperature, which was due to the particle sintering during calcination at high temperature [1]. The physical-adsorption results revealed that the improved method offered material with higher surface area and more mesopores.

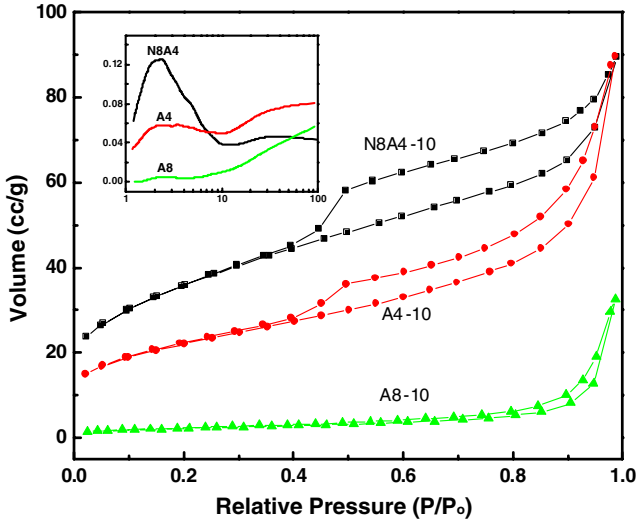

Fig. 2. N_2 adsorption–desorption isotherms and the pore size distributions of samples N8A4, A4 and A8.

Table 1
Surface areas, mean crystallite sizes and lattice parameters of $Ce_{0.9}Cu_{0.1}O_{2-\delta}$ catalysts

Sample	Surface area ($m^2\,g^{-1}$)	Mean crystallite size (nm)	Lattice parameter (nm)
N8A4	131	7.2	0.5410
A4	60	9.5	0.5410
A8	10	53.4	0.5406

XRD patterns of $Ce_{0.9}Cu_{0.1}O_{2-\delta}$ solid solutions prepared by two methods were presented in Fig. 3. The typical diffraction peaks of CeO_2 were observed in all the samples. Weak diffraction peaks of CuO phase appeared only in sample A8, which indicated that CuO species was finely dispersed on the surface of sample N8A4 and A4. The mean crystallite sizes of all samples calculated by the Scherrer equation were listed in Table 1. The crystallite size of N8A4, A4 and A8 is 7.2 nm, 9.5 nm and 53.4 nm, respectively. Obviously, the improved citrate sol–gel method could offer the catalyst with smaller crystallite size. For the conventional method, the particles underwent sintering at high calcination temperature [17], which might be the reason that the A8 had the largest crystallite size. The incorporation of thermal treatment under N_2 atmosphere, even at 800 °C, was favorable for the small crystallite size, which was consistent with the results reported by Xie et al. [2].

The lattice parameters of the samples are also listed in Table 1. All of them were smaller than that of pure CeO_2 (0.5424 nm). This is because the radius of Cu^{2+}(0.079 nm) is smaller than that of Ce^{4+}(0.092 nm) [18], which leads to the shrink of CeO_2 lattice when $Ce^{4+}$was partially substituted with Cu^{2+}. This indicated that the $Ce_{0.9}Cu_{0.1}O_{2-\delta}$ solid solution was formed in these catalysts [19].

Fig. 4 shows H_2-TPR profiles of $Ce_{0.9}Cu_{0.1}O_{2-\delta}$ solid solutions. From the figure, it could be seen that three reduction peaks (α, β and θ) appeared in both profiles of N8A4 and A4, these peaks were at about 204 °C (α), 240 °C (β) and 850 °C (θ), respectively. The position of low-temperature reduction peak of A4 shifted to higher temperature about 10 °C compared to N8A4. However, the A8 shows only two peaks: one was low-temperature reduction peak centered at 380 °C (γ), the other was high-temperature reduction peak centered at 830 °C (θ). The reduction temperature of peak γ was obviously higher than

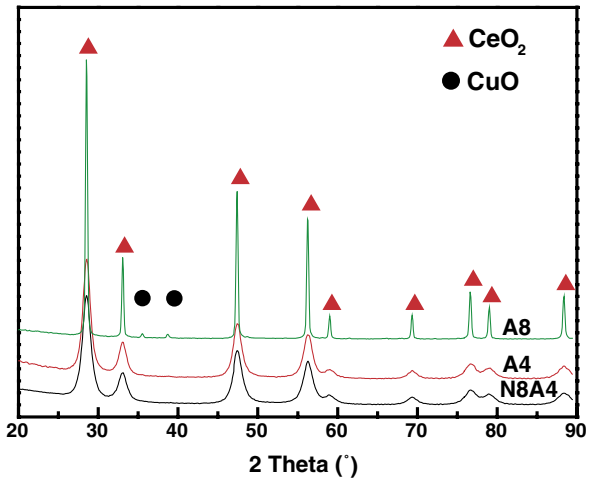

Fig. 3. XRD patterns of samples N8A4, A4 and A8.

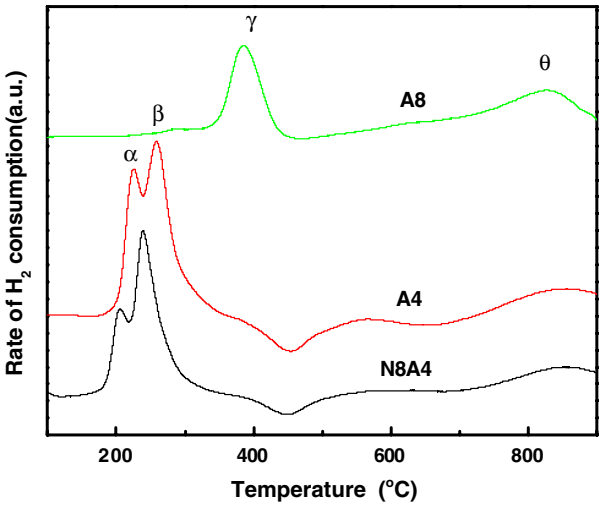

Fig. 4. H_2-TPR profiles of samples N8A4, A4 and A8.

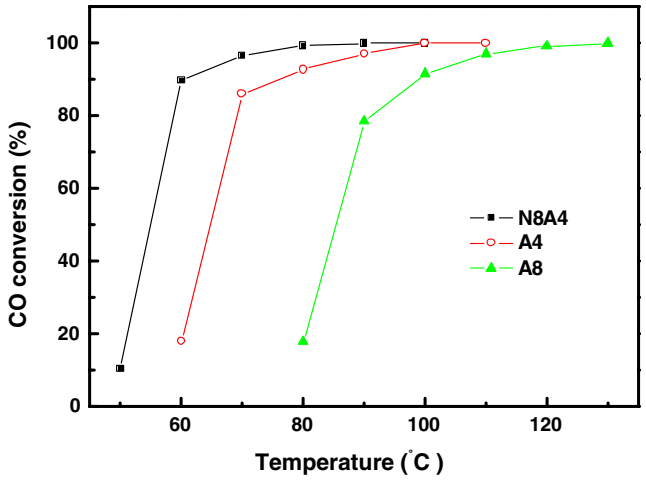

Fig. 5. Catalytic activities of samples N8A4, A4 and A8 for CO oxidation.

that of peak α and β, indicating that the process of preparation and the way of calcination influence the redox properties of catalysts distinctively.

According to the literature [20], the peak θ was attributed to the reduction of partial surface oxygen on CeO_2. Since no significant difference in the position of peak θ for the three samples, it was not discussed here. Compared with the sample A4, the low-temperature reduction peaks of sample N8A4 shifted to lower temperature, probably due to the sample with higher surface area and smaller crystallite size that was easier to be reduced, which was reported by George Avgouropoulos [9]. The peak α was ascribed to the reduction of finely dispersed CuO species on the surface of solid solution, while peak β was due to the reduction of bulk CuO phase [21]. However, from XRD patterns, it was found that the $Ce_{0.9}Cu_{0.1}O_{2-\delta}$ solid solution was formed, thus there was Cu^{2+} penetrated into the CeO_2 lattice certainly other than the finely dispersed CuO species. It was inevitable that a small amount of larger bulk CuO particle existed on the surface. As above mentioned, we believe that peak α was attributed to the reduction of finely dispersed CuO species on the surface of solid solution, while peak β was due to the reduction of Cu^{2+} penetrated into the CeO_2 lattice or a little larger bulk CuO particle.

For the sample A8, the peak α and β disappeared and only peak γ was observed. The disappearance of peak α was due to the finely dispersed CuO species aggregated larger bulk CuO phase when the catalyst was calcined at 800 °C, which was consistent with the XRD results. The reduction temperature of Cu^{2+} penetrated into the CeO_2 lattice or bulk CuO particle increased significantly with the disappearance of peak α. It was because that the finely dispersed CuO species was easily reduced to metallic Cu when peak α was present. And the effect of hydrogen spillover on the metallic Cu resulted in the decrease of the reduction temperature of other CuO species. Therefore, the disappearance of peak α was the reason of peak β shifted to higher temperature (peak γ), which was in agreement with Jung et al. [22]. That is to say, peak γ was also ascribed to the reduction of Cu^{2+} species that penetrated into the CeO_2 lattice or to the reduction of larger bulk CuO phase.

3.2. Activity of CO oxidation at low temperature

Fig. 5 shows the catalytic activities of $Ce_{0.9}Cu_{0.1}O_{2-\delta}$ solid solutionsfor CO oxidation. The T_{90} (the temperature when the conversion is 90%) for the samples N8A4, A4 and A8 were 60 °C, 80 °C, and 100 °C, respectively. It was clear that the sample N8A4 had better activity than the other two. Additionally, the surface areas of N8A4, A4 and A8 were 131 $m^2\,g^{-1}$, 60 $m^2\,g^{-1}$ and 10 $m^2\,g^{-1}$, respectively. Obviously, the higher the surface area was, the better catalytic activity. The catalysts with higher surface area could provide more active species [1], which could decrease the reaction temperature and enhance the activity. Considering the TPR results, it was found that the better catalytic activity of N8A4 was also due to lower temperature of peak α. Compared sample A4 with A8, A4 shows better activity than A8, which also could be attributed to the existence of the peak α. As mentioned before, this peak α could be ascribed to the reduction of the finely dispersed CuO on the surface of solid solution, which was easier to be reduced at low temperature. Therefore, it could be concluded that the finely dispersed CuO species on the surface of solid solution was the active site for low temperature CO oxidation.

4. Conclusion

The improved citrate sol–gel method can afford the fluorite-like cubic $Ce_{0.9}Cu_{0.1}O_{2-\delta}$ solid solution with nanoparticles of 7.2 nm and high specific surface area of 131 $m^2\,g^{-1}$. The incorporation of thermal treatment under N_2 atmosphere can prevent small crystallite size from sintering and afford a high surface area carrier, thus induces the CuO species to finely dispersed phase, so enhances

the catalytic activity for low temperature CO oxidation. The finely dispersed CuO species on the surface of solid solution is responsible for low temperature CO oxidation.

Acknowledgement

This work is financially supported by the Natural Science Foundation of China (Grant 20473075).

References

[1] W.H. Shen, X.P. Dong, Y.F. Zhu, H.R. Chen, J.L. Shi, Microporous Mesoporous Mater. 85 (2005) 157.
[2] G.Q. Xie, M.F. Luo, M. He, P. Fang, J.M. Ma, Y.F. Ying, Z.L. Yan, J. Nanopart. Res. 3 (2006), doi:10.1007/s11051-005-9052-7.
[3] X.L. Tang, B.C. Zhang, Y. Li, Y.D. Xu, Q. Xin, W.J. Shen, Catal. Today 93–95 (2004) 191.
[4] B. Skarman, D. Grandjean, R.E. Benfield, A. Hinz, A. Andersson, L.R. Wallenberg, J. Catal. 211 (2002) 119.
[5] Y.H. Hu, L. Dong, J. Wang, W.P. Ding, Y. Chen, J. Mol. Catal. A: Chem. 162 (2000) 307.
[6] Y. Liu, Q. Fu, M.F. Stephanopoulos, Catal. Today 93–95 (2004) 241.
[7] X.C. Zheng, D.Z. Han, S.P. Wang, S.M. Zhang, S.R. Wang, W.P. Huang, S.H. Wu, J. Rare Earth. 23 (2005) 47.
[8] G. Sedmak, S. Hocevar, J. Levec, J. Catal. 213 (2003) 135.
[9] G. Avgouropoulos, T. Ioannides, Appl. Catal. A 244 (2003) 155.
[10] M.F. Luo, Y.J. Zhong, X.X. Yuan, X.M. Zheng, Appl. Catal. A 162 (1997) 121.
[11] J.E. Spanier, R.D. Robinson, F. Zhang, S.W. Chan, I.P. Herman, Phys. Rev. B 64 (2001) 245407.
[12] C. Ho, J.C. Yu, T. Kwong, A.C. Mak, S. Lai, Chem. Mater. 17 (2005) 4514.
[13] S. Carrettin, P. Concepcion, A. Corma, J.M. Lopez Nieto, V.F. Puntes, Angew Chem. Int., Ed. 43 (2004) 2538.
[14] N. Phonthammachai, M. Rumruangwong, E. Gulari, A.M. Jamieson, S. Jitkarnka, S. Wongkasemjit, Colloids Surf. A 247 (2004) 61.
[15] L.M. Chen, X.M. Sun, Y.N. Liu, Y.D. Li, Appl. Catal. A 265 (2004) 123.
[16] A.R. Liu, S.M. Wang, Y.R. Zhao, Z. Zheng, Mater. Chem. Phys. 99 (2006) 131.
[17] A. Bumajdad, M.I. Zaki, J. Eastoe, L. Pasupulety, Langmuir 20 (2004) 11223.
[18] J.A. Dean (Ed.), Lang's Handbook of Chemistry, 23rd ed., McGraw-Hill, New York, 1985, p. 3.
[19] W.J. Shan, Z.C. Feng, Z.L. Li, J. Zhang, W.J. Shen, C. Li, J. Catal. 228 (2004) 206.
[20] X.C. Zheng, X.L. Zhang, Z.Y. Fang, X.Y. Wang, S.R. Wang, S.H. Wu, Catal. Commun. 7 (2006) 701.
[21] X.Y. Jiang, G.L. Lu, R.X. Zhou, J.X. Mao, Y. Chen, X.M. Zheng, Appl. Surf. Sci. 173 (2001) 208.
[22] C.R. Jung, J. Han, S.W. Nam, T.H. Lim, S.A. Hong, H.I. Lee, Catal. Today 93–95 (2004) 183.